The All-fiber MZI Structure for Optical DPSK Demodulation and Optical PSBT Encoding

Guillaume Ducournau, Olivier Latry and Mohamed Ketata
LEMI, Laboratoire Electronique Microtechnologie et Instrumentation
IUT-LEMI 76821 Mont Saint Aignan, France
guillaume.ducournau@univ-rouen.fr

ABSTRACT

Since the beginning of optical telecommunications, the most simple modulation format has been employed in optical links. This format is called OOK (On Off Keying). With the increases in bit rates, number of optical channels in Dense Wavelength Division Multiplexing (DWDM) configuration, and the augmentation of power in each channel, new modulation formats have been studied in the last years. Today, in order to increase the quality of optical links, tendency is to modify the modulation scheme used to encode information in light signals. Particularly, the Differential Phase Shift Keying (DPSK) format presents an increased tolerance to non-linear effects in optical fibers, justifying the interest for using this format in optical communications links.
In the past two years, some studies investigated the possibilities to transmit 40 Gbps data rates on the deployed 10 Gbps links. An interesting solution consists in using the Phase Shaped Binary Transmission (PSBT) modulation format. With this technique, the system upgrade costs from 10 Gbps to 40 Gbps are reduced, justifying the use of PSBT.
In this paper, we present two applications of Mach-Zehnder Inteferometers (MZIs), used in optical communication links. We first review the principles of the Differential Phase Shift Keying (DPSK), a phase modulation scheme, and its interest in optical communications. After that, we also focus on a recently introduced modulation format: the all-optical Phase Shaped Binary Transmission (PSBT).

Keywords: Optical Communications, Modulation formats, DPSK, PSBT, Mach-Zehnder Interferometer (MZI).

1. INTRODUCTION

Today, most of the optical telecommunication links use the well known modulation format called OOK (On Off Keying). Due to the increases in bit rates, power and number of DWDM channels, the OOK format reaches its limits for optical communications. Various modulation schemes have already been used in the electrical domain during last decade, but have not been applied in optics. Recently the use of new modulation formats in optical communications has been considered and compared for increasing the tolerance of the optical link to impairments such as chromatic dispersion, PMD or non-linearity (Kerr Effect) [1-3].

Among the various modulation formats, we present here the Differential Phase Shift Keying (DPSK) scheme and the Phase Shaped Binary Transmission (PSBT). DPSK presents a better robustness to optical non-linearities than the classical OOK, particularly for the Cross Phase Modulation (XPM) in DWDM systems [1]. It has also been shown that DPSK format has better performances due to PMD degradations than the classical OOK [2]. The disadvantage of the DPSK is that a direct detection (DD) at the end of the optical link is not possible, since DPSK is a phase modulation. An interferometric demodulation stage must be inserted in front of the photo-detection. This stage is an "Add and Delay" structure, which is composed by a MZI. In this structure, one arm presents an optical delay line equal to the bit duration. This MZI converts an optical DPSK to an intensity-modulated (IM) signal, followed by a DD.

The PSBT format is encoded from a DPSK: first a DPSK signal is generated and after that a MZI structure converts the DPSK to an intensity-modulated signal: the PSBT. MZI characteristics for the two applications are slightly different, as we will see in the next sections.

The paper is organised as follows: we first describe the principles of the DPSK and PSBT modulation schemes. After that, the MZI structure is detailed (section 4). The section 5 focuses on experimental aspects for MZI characterization and section 6 deals with the evaluation of the required performances for a MZI used as a DPSK demodulator. In section 7, a system implementation of an all-fiber MZI in a 43 Gbps optical link is presented, and the some of the characteristics required for MZI used for PSBT encoding.

2. PRINCIPLES OF DPSK MODULATION SCHEME

Modulation
In the paper, T_b denotes the time duration of one bit, and t is the time. Moreover, we depicted here for convenience the case of NRZ (Non Return Zero) signals. For further information about modulations formats, see [3]. The well-known OOK format is a simple binary modulation of light: a "1" is represented by presence of optical signal, and "0" by no signal. This is not the case for DPSK, where optical signal is always present in the fiber. The information is differentially encoded in the phase of the light: a precode c(k) is produced with the message m(k) according to the following rule :

$$c(k) = \overline{m(k) \oplus c(k-1)} \qquad (1)$$

where k is the integer part of t/T_b.
$\oplus$ represents the xor logic operation.
The binary sequence c(k) drives a phase modulator, where a π phase shift is applied when c(k) = 1, and no phase shift if c(k) = 0. To summarize this, we can write the form of electrical fields in case of OOK and DPSK:

$$E_{OOK} = m(k).E_0.\cos(\omega_0.t) \quad (2)$$

$$E_{DPSK} = E_0.\cos(\omega_0.t + \underbrace{c(k).\pi}_{\Delta\varphi(k)}) \quad (3)$$

The binary information (data) is carried by amplitude in the OOK modulation scheme, and by phase with DPSK. Waveforms of the fields are represented in Figure 1. CW stands for Continuous Wave, and represents the optical carrier.

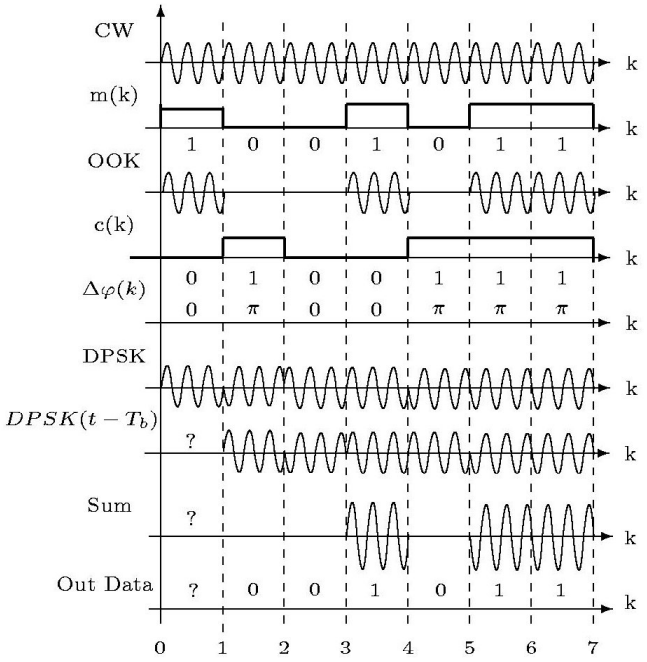

Figure 1. Waveforms of electrical fields, and principle of DPSK demodulation.

Demodulation

In order to recover the binary information (message m(k)) carried by OOK signal, a simple photo-diode can be used, this is the Direct Detection (DD). This is not the case for DPSK, where binary "1" and "0" have the same optical powers. A photo-diode can't differentiate the two logic levels, and a demodulation stage is needed, to transform the phase modulated to an intensity modulated signal, followed by DD. The demodulation operation consists in a summation of the DPSK signal and the same delayed by the bit-duration T_b, as indicated in Figure 1 for DPSK(t-T_b) and Sum signals. This demodulation stage is the MZI, and operation will be depicted in part 3. Here we note that when demodulating a DPSK signal, the first binary value is arbitrary, and an initialisation sequence will be necessary for transmission.

DPSK Transmitter

First of all, NRZ-OOK is classically obtained with a Mach-Zehnder Modulator (MZM) biased at half power of the transmission curve and driven with a Vπ amplitude signal [4]. RZ formats are then obtained with the pulse carving summarized in Figure 2. For DPSK signal generation, the MZM is driven in a push-pull configuration and biased at the minimum transmission curve, as presented in [4]. Finally, insets of the Figure 2 shows the eye diagrams obtained with these various modulation formats.

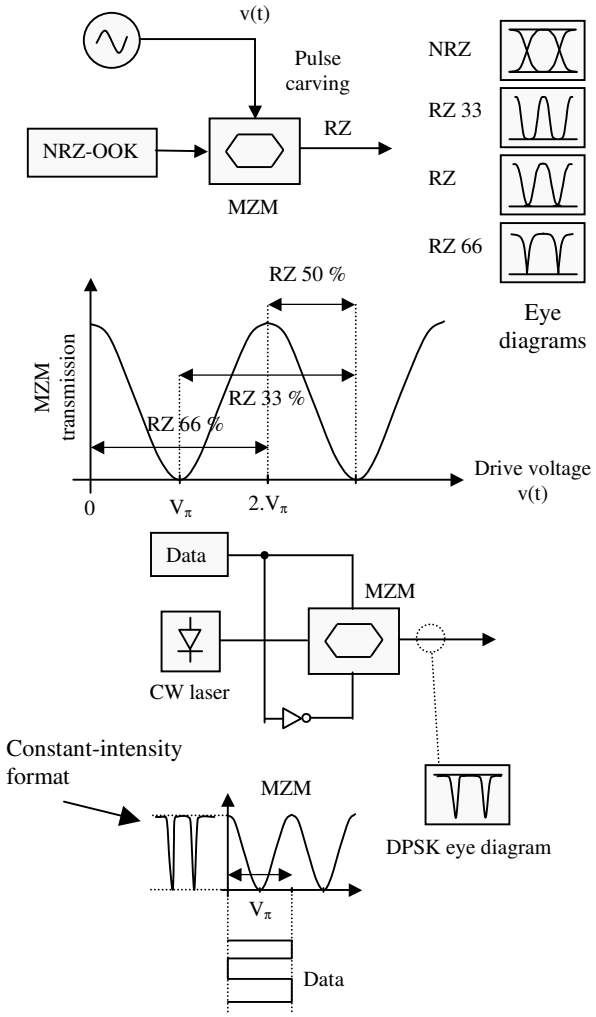

Figure 2. OOK and DPSK transmitters and pulse Carving for RZ codes generation.

As the DPSK format is a constant-intensity format, the non linear index modulation (Kerr effect) is reduced, resulting as a better robustness to non linear effects occurring during the propagation in optical fibers.

3. PRINCIPLES OF THE PSBT MODULATION SCHEME

The second modulation format considered here is the "Phase Shaped Binary Transmissions", optically encoded. Electrical PSBT has been proposed for the first time in [5]. It consists in driving Mach Zehnder Modulators (MZM) with electrical NRZ signals filtered by an appropriate Bessel filter. This ensures a superimposed phase modulated signal in addition to the conventional amplitude signal shape. This amplitude/phase profile leads to an increased robustness towards group velocity dispersion (GVD) in optical fibers. Electrical PSBT signal is also often denoted as duobinary signal due to the reduced-size spectrum obtained.

Electrical PSBT has been theoretically demonstrated in [6] and after that experimental work [7, 8] confirmed the superior chromatic dispersion tolerance of PSBT versus conventional

NRZ signals. All optical solution for PSBT generation have been proposed in [9]. This solution has been experimentally demonstrated to ensure a higher tolerance to GVD than conventional NRZ, but less GVD robustness than electrical PSBT generation.

The all optical PSBT solution presents a very attractive characteristic: one optical filter (Mach Zehnder Interferometer, MZI) is needed for all ITU channels, due to the fact that the MZI has a Free Spectral Range (FSR) equal to the ITU grid spacing. This WDM compliance is an advantage over electrical PSBT, which requires n Bessel filters for n channels encoding.

All-optical PSBT is obtained with partial DPSK demodulation with MZI filter [9] and reported in Figure 3.

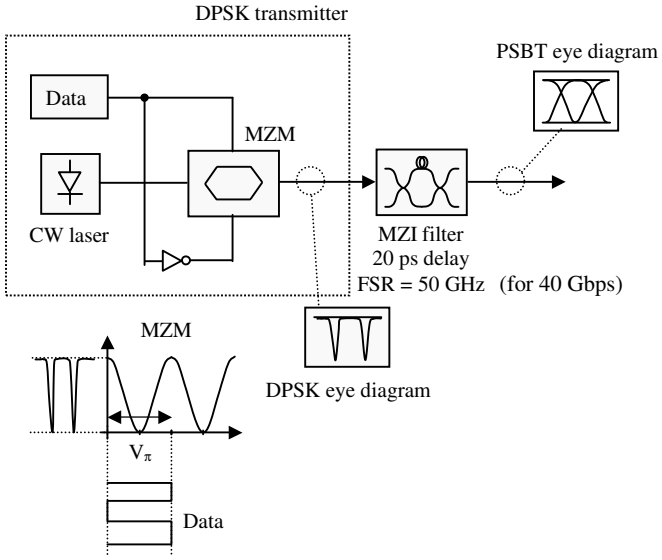

Figure 3. PSBT transmitter.

4. THE MZI STRUCTURE

We have seen that DPSK and PSBT can offer improved performances but an interferometric conversion is needed. As explained in section 2, the principle of DPSK demodulation is a time superposition of optical electric field and the same delayed by the bit duration (T_b). The optical circuit used for realizing this operation is shown in Figure 4. A 3 dB optical coupler is used for separation of optical electric field between two arms. One arm has a superior fiber length ΔL for delaying optical signal by T_b. Then a second 3 dB optical coupler combines the optical power at the end of the two arms.

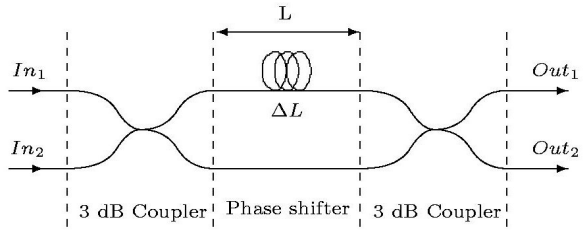

Figure 4. 4-Ports MZI structure.

Without taking into account any polarization effects, a possible approach to describe the transfer function of the device is to use the transfer matrix theory [10]. In this theory, 2*2 matrices are used to represent transformation of fields:

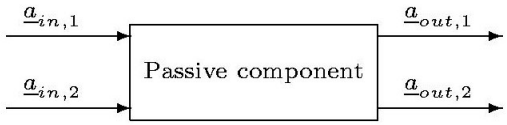

Figure 5. Two ports optical device.

The relation between in and out ports of the passive device is written as (5):

$$\begin{pmatrix} \underline{a}_{out,1} \\ \underline{a}_{out,2} \end{pmatrix} = \underbrace{\begin{pmatrix} m_{11} & m_{12} \\ m_{21} & m_{22} \end{pmatrix}}_{M} \begin{pmatrix} \underline{a}_{in,1} \\ \underline{a}_{in,2} \end{pmatrix} \quad (5)$$

Optimal MZI device

For an ideal 3 dB optical coupler (50/50 coupling ratios), the transfer matrix M_{3dB} is:

$$M_{3dB} = \frac{1}{\sqrt{2}} \begin{pmatrix} 1 & j \\ j & 1 \end{pmatrix} \quad (6)$$

Where $j^2 = -1$. In this coupler, 50% of power in each input port is coupled in the output ports. For a phase shifter device, the transfer matrix is:

$$M_{\Delta\varphi} = \begin{pmatrix} e^{j.\Delta\varphi_1} & 0 \\ 0 & e^{j.\Delta\varphi_2} \end{pmatrix} = e^{j.\Delta\varphi_2} \begin{pmatrix} e^{j.\Delta\varphi} & 0 \\ 0 & 1 \end{pmatrix} \quad (7)$$

where: $\Delta\varphi = \Delta\varphi_1 - \Delta\varphi_2$, represents the phase imbalance between two arms, and $\Delta\varphi_1$, $\Delta\varphi_2$ stand for the supplementary optical phases when electric fields travelled along the upper arm or in the other, respectively. Here, in the phase shifter of Figure 4, and $\Delta\varphi_1$ and $\Delta\varphi_2$ are:

$$\Delta\varphi_1 = \beta.(L + \Delta L) \text{ and } \Delta\varphi_2 = \beta.L \quad (8)$$

where β is the propagation constant of the guided mode along the fiber. The supplementary length of fiber ΔL in the upper arm has to delay electrical field by the bit duration T_b, so we can write:

$$\Delta\varphi = \beta\Delta L = \omega.T_b \quad (9)$$

where ω is the optical frequency.

Typical bit rates are 10, 20 and 40 Gbps. For these three values, table 1 gives the supplementary length ΔL needed between two arms of MZI for DPSK demodulation. We use classical SMF 28 fiber with following parameters:

$n_{core} = 1.4675$, $n_{cladding} = 1.46422$, $r_{core} = 4.5$ μm, $r_{cladding} = 62.5$ μm.

Bit rate (Gbit/s), FSR (GHz)	10	20	40
Bit duration Tb (ps)	100	50	25
ΔL (cm)	2,046	1,023	0,511

Table 1. Values of supplementary length ΔL in one arm.

With Eq. (6) and Eq. (7), the total transfer matrix of the MZI device is:

$$M_{MZI} = M_{3dB}.M_{\Delta\varphi}.M_{3dB}$$

$$M_{MZI} = \frac{e^{j\Delta\varphi_2}}{2} \begin{pmatrix} e^{j\Delta\varphi} - 1 & j.\left(e^{j\Delta\varphi} + 1\right) \\ j.\left(e^{j\Delta\varphi} + 1\right) & 1 - e^{j\Delta\varphi} \end{pmatrix} \quad (10)$$

For DPSK demodulation, the optical field is inserted in input port 1, and the second input port have no signal. The output fields amplitudes can be written as:

$$\begin{pmatrix} \underline{a}_{out1} \\ \underline{a}_{out2} \end{pmatrix} = M_{MZI} . \begin{pmatrix} \underline{a}_{in1} \\ 0 \end{pmatrix}$$

$$\begin{cases} \underline{a}_{out1} = \dfrac{e^{j\Delta\varphi_2}}{2} . \left(e^{j\Delta\varphi} - 1\right) \underline{a}_{in1} \\ \underline{a}_{out2} = \dfrac{e^{j\Delta\varphi_2}}{2} . j . \left(e^{j\Delta\varphi} + 1\right) \underline{a}_{in1} \end{cases} \quad (11)$$

If an optical field modulated in DPSK format is injected in port In1, we have:

$$\begin{cases} \underline{a}_{out1} = \dfrac{e^{j\Delta\varphi_2}}{2} . \left(e^{j\omega T_b} - 1\right) \underline{a}_{DPSK}(t) \\ \underline{a}_{out2} = \dfrac{e^{j\Delta\varphi_2}}{2} . j . \left(e^{j\omega T_b} + 1\right) \underline{a}_{DPSK}(t) \end{cases} \quad (12)$$

$$\begin{cases} \underline{a}_{out1} = \dfrac{e^{j\Delta\varphi_2}}{2} . \left(\underline{a}_{DPSK}(t - T_b) - \underline{a}_{DPSK}(t)\right) \\ \underline{a}_{out2} = \dfrac{e^{j\Delta\varphi_2}}{2} . j . \left(\underline{a}_{DPSK}(t - T_b) + \underline{a}_{DPSK}(t)\right) \end{cases} \quad (13)$$

In Eq. (13), we see that the port Out2 of MZI structure realizes the DPSK demodulation. The output field is equal to the sum of DPSK signal and the same, delayed by T_b. The Out2 port is denoted as "constructive port". The other out port is called "destructive port". For evaluation of power transmission in the two output ports, the optical powers ($P = K.\underline{a}.\underline{a}^*$, where * is the complex conjugate) of the device can be written as:

$$\begin{cases} P_{out1} = \dfrac{1}{4} . \left(e^{j\omega T_b} - 1\right)\left(e^{-j\omega T_b} - 1\right) . P_{in1} \\ P_{out2} = \dfrac{1}{4} . \left(e^{j\omega T_b} + 1\right)\left(e^{-j\omega T_b} + 1\right) . P_{in1} \end{cases} \quad (14)$$

$$\begin{cases} T_1 = \dfrac{P_{out1}}{P_{in1}} = \dfrac{1}{2} . \left(1 - \cos(2.\pi.\nu.T_b)\right) \\ T_2 = \dfrac{P_{out2}}{P_{in1}} = \dfrac{1}{2} . \left(1 + \cos(2.\pi.\nu.T_b)\right) \end{cases} \quad (15)$$

where $\omega = 2.\pi.\nu$, and ν is the optical frequency.

These two last expressions bring definition of four parameters for the MZI. First, the FSR (Free Spectral Range) is defined as the spectral period of transmission spectrum. The differential delay T_b is then equal to 1/FSR. Three, the Insertion loss (IL) of MZI will be the absolute max value of transmission in dB scale, in each port. For an ideal MZI, the IL is 0 dB in two ports. Last, the isolation of MZI will be the gap between maximal and minimal transmission values of the spectrum, also in each port. Here, the minimal transmission is 0 (-∞ dB) and the maximum is 1 (0 dB). The ideally isolation for the two ports is ∞. The power transmission in dB scale of the two output ports are represented in Figure 6. Frequency values are chosen from 193.25 THz to 193.55 THz, corresponding to the ITU channels 24 to 26.

Non optimal MZI

The isolation of MZI device is a critical parameter for DPSK demodulation because logical "0" are created by destructive interferences at an output port. If the contrast of interference is not optimal (equals to 1 ideally, corresponding to an infinite isolation), the demodulated "0" will contain optical power, then the OSNR (Optical Signal to Noise Ratio) will be reduced, and the BER as well. There are three sources which can affect the isolation value: non ideal couplers, an arm containing more optical losses than the other, and the MZI dependence to polarisation.

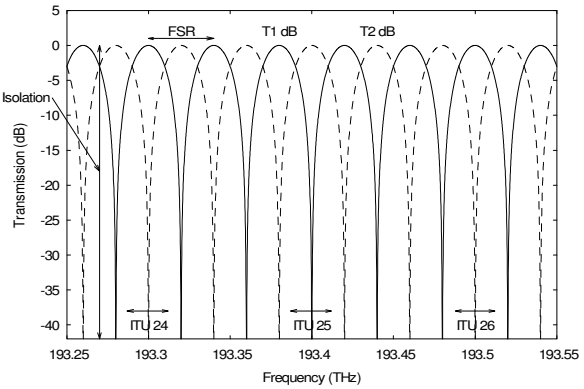

Figure 6. Power transmission of ideal MZI. T_b = 25 ps, FSR = 40 GHz. Isolation = ∞. Solid curve: T_1 dB and dashed curve T_2 dB.

Transmission spectra of non-ideal MZIs

The transmissions T1 and T2 for the two output take a different form from Eq. (15). For an optical coupler with a_1^2/b_1^2 coupling ratios, the transfer matrix can be written as Eq. (16) [10]. Adding a loss in one of the two arms, the phase shifter's matrix became Eq. (17):

$$M_{coupler} = \begin{pmatrix} a_1 & j.b_1 \\ j.b_1 & a_1 \end{pmatrix} \quad (16)$$

with $a_1^2 + b_1^2 = 1$.

$$M'_{\Delta\varphi} = \begin{pmatrix} e^{j.\Delta\varphi_1} & 0 \\ 0 & \alpha.e^{j.\Delta\varphi_2} \end{pmatrix} = e^{j.\Delta\varphi_2} \begin{pmatrix} e^{j.\Delta\varphi} & 0 \\ 0 & \alpha \end{pmatrix} \quad (17)$$

where α takes places for the optical loss in the under arm.

The total transfer matrix is calculated as previous, leading to:

$$M'_{MZI} = e^{j\Delta\varphi_2} \begin{pmatrix} a_2 & j.b_2 \\ j.b_2 & a_2 \end{pmatrix} . \begin{pmatrix} e^{j\Delta\varphi} & 0 \\ 0 & \alpha \end{pmatrix} . \begin{pmatrix} a_1 & j.b_1 \\ j.b_1 & a_1 \end{pmatrix} \quad (18)$$

$$M'_{MZI} = e^{j\Delta\varphi_2} \begin{pmatrix} a_2.a_1.e^{j\Delta\varphi} - \alpha.b_2.b_1 & j.\left(a_2.b_1.e^{j\Delta\varphi} + \alpha.b_2.a_1\right) \\ j.\left(a_1.b_2.e^{j\Delta\varphi} + \alpha.b_1.a_2\right) & \alpha.a_2.a_1 - b_2.b_1.e^{j\Delta\varphi} \end{pmatrix}$$

where the index i in a_i and b_i denotes the i^{th} coupler of MZI device. For an ideal MZI, we take a_1, a_2, b_1 and b_2 equal to $1/\sqrt{2}$, and $\alpha = 1$. T1 and T2 become:

$$\begin{cases} T'_1 = a_1^2.a_2^2 + b_1^2.b_2^2.\alpha^2 - 2.a_1.a_2.b_1.b_2.\alpha.\cos(2.\pi.\nu.T_b) \\ T'_2 = a_1^2.b_2^2 + b_1^2.a_2^2.\alpha^2 + 2.a_1.a_2.b_1.b_2.\alpha.\cos(2.\pi.\nu.T_b) \end{cases} \quad (19)$$

With Eq. (19) we can write the isolation value in each port:

$$Isolation_{i,dB} = 10.\log\left[\frac{T'_{i\max}}{T'_{i\min}}\right]$$

$$Isolation_{1,dB} = 10.\log\left[\left(\frac{a_1.a_2 + b_1.b_2.\alpha}{a_1.a_2 - b_1.b_2.\alpha}\right)^2\right]$$

$$Isolation_{2,dB} = 10.\log\left[\left(\frac{a_1.b_2 + b_1.a_2.\alpha}{a_1.b_2 - b_1.a_2.\alpha}\right)^2\right] \quad (20)$$

The insertion loss of a non ideal MZI is not equal to 0 dB, and will be different for the two output ports:

$$IL_{1,dB} = \left|10.\log\left(a_1.a_2 + b_1.b_2.\alpha\right)^2\right|$$

$$IL_{2,dB} = \left|10.\log\left(a_1.b_2 + b_1.a_2.\alpha\right)^2\right| \quad (21)$$

On practical MZIs, IL_i can be wavelength dependent. The uniformity is then defined as the maximum difference between IL_i at different wavelengths. In Figure 7, we plot transmission for non-ideal couplers (coupling ratios a_1^2/b_1^2 different from 50/50), without optical losses in under arm. With Eq. (21), the IL is 0 dB. In Figure 8, we plot transmission for ideal couplers, with an under arm loss of 0.45 dB ($\alpha = 0.95$). The IL equals to 0.22 dB in two ports, and we can verify on the graph that maximal transmission is not 0 dB. The Figures 7 and 8 show that a default in coupling ratio (not exactly equal to 50/50), and the presence of a loss in under arm affect the quality of interference: isolations values are degraded.

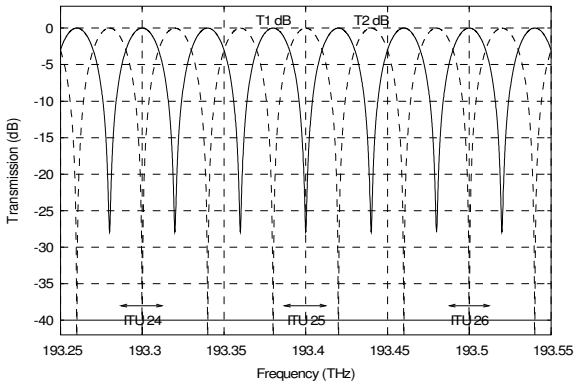

Figure 7. Power spectrum of a non-ideal MZI: the coupling ratio of optical couplers is 52/48. Here $\alpha = 1$ (no losses in under arm). $Isolation_1 = 27.96$ dB, $Isolation_2 = \infty$. $IL_1 = 0$ dB. $IL_2 \approx 0$ dB.

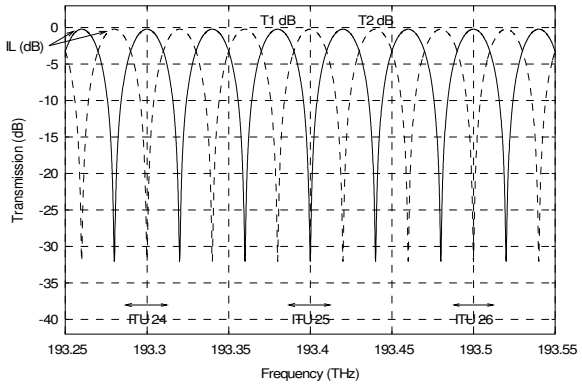

Figure 8. Power spectrum of a non-ideal MZI: the coupling ratio of couplers is 50/50, and with an under arm loss of 0.45 dB. $Isolation_1 = Isolation_2 = 31.82$ dB. $IL = IL_1 = IL_2 = 0.22$ dB.

In Figures 9 and 10, we plot the degradation of isolations versus evolution of coupling ratios a_1^2 and a_2^2, and also with α.

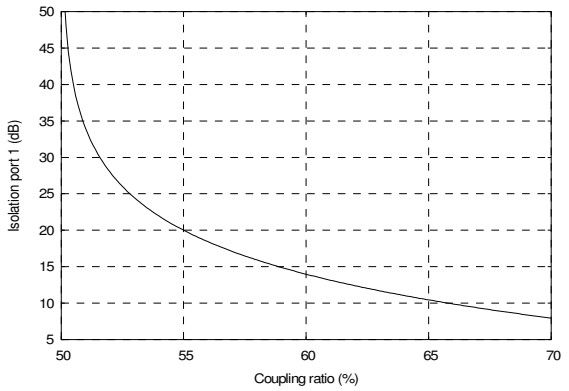

Figure 9. Evolution of isolation in port 1 versus coupling ratio $a_1^2 = a_2^2$. Isolation in port 2 is infinite, due to $\alpha = 1$.

If the two effects (coupling ratios different from 50/50 and loss in under arm) add themselves, the value of isolations are given by Eq. (20). With these expressions, we can say that isolation can't be infinite at the same time for the two output ports. Moreover, isolations in two ports are not equal. This will be a source of BER degradation when using balanced photo-detection, but it will not be studied here. For exemple, the transmission spectra of a MZI with two defaults is plotted in Figure 11.

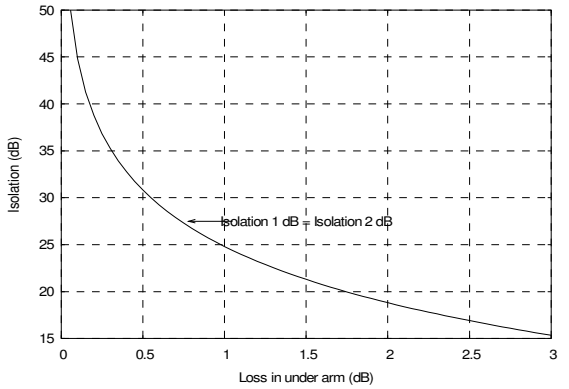

Figure 10. Evolution of Isolation in two ports versus α (loss in under arm). The coupling ratios are 50/50.

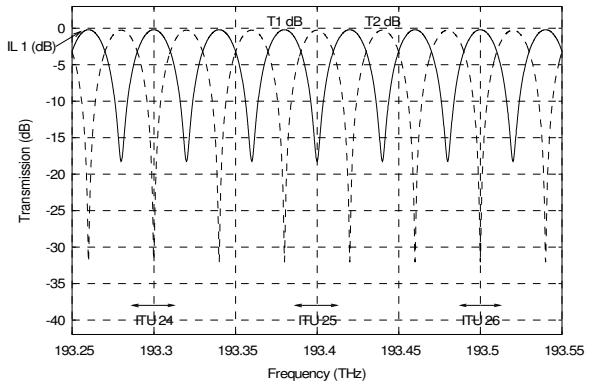

Figure 11. Transmission spectra of MZI with two defaults: coupling ratios 55/45, and 0.45 dB under arm loss. $Isolation_1 = 18.04$ dB, $Isolation_2 = 31.82$ dB. $IL_1 = 0.198$ dB, $IL_2 = 0.265$ dB.

We now focus on the port 2, which realizes DPSK demodulation. In Figure 12 we plotted insertion loss surface in port 2 versus α_{dB} and coupling ratio a_1^2.

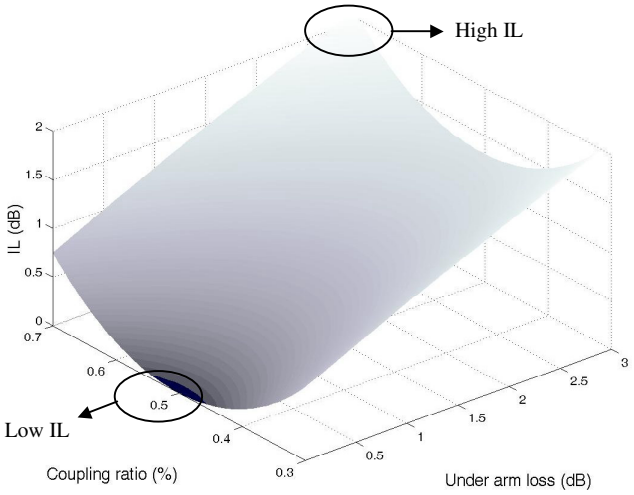

Figure 12. Evolution of IL with coupling ratio a_1^2 and arm loss α dB.

As can be seen, port 2 has no IL when arms are lossless and with 50/50 coupling ratios. The Insertion loss increases with losses in under arm and with default in coupling ratios. We can conclude on study of IL and isolation by saying: Practical MZIs should have low ILs and high isolation in port 2, and this may be obtained by combining coupling ratios 50/50, and a low loss in under arm.

Influence of polarisation

We said that the MZI was polarisation sensitive: when light travels in two arms, polarisation is randomly fluctuating. At the second optical coupler, it is highly probable that polarisations of fields in two arms will be different, and the interference will not be completely destructive. A few part of optical power will be transmitted and the isolation value will be degraded by this way. In order to reduce these isolations degradations, the lengths of the two arms has to be as small as possible, without any mechanical constrains, or as small as possible.

MZI thermal drift

If the interferometer is in a variable temperature (written as T in (23)) environment, two effects will induce a frequency shift on the interferometer transmission spectra: the thermo-optic effect and the thermal expansion effect. The thermo-optic effect modifies the value of the core index, resulting in a variation of the effective index δneff, thus inducing a variation of the propagation constant δβ. Thermal expansion effect implies a phase variation induced by the differential length variation δ(ΔL). The variation of the differential phase between the two arms obtained by these two effects is finally given by (23).

$$\Delta\varphi = \beta.\Delta L \Rightarrow \delta(\Delta\varphi) = \underbrace{\delta\beta.\Delta L}_{T.O.E.} + \underbrace{\beta.\delta(\Delta L)}_{T.E.E.} \quad (22)$$

$$\delta(\Delta\varphi) = \frac{2.\pi}{\lambda}.\delta n_{eff}.\Delta L + \beta.\alpha_t.\Delta L.\delta T \quad (23)$$

In (3), αt is the thermal expansion coefficient, equal to 0.55*10-6 K^{-1} for the single mode fiber (SMF) 28. The effective index variation due to a small thermal shift δT is δneff, and the wavelength is λ.

The calculus of δn_{eff} is obtained with the first order approximation $\delta n_{core/cladding} = \chi_t \cdot n_{core/cladding} \cdot \delta T$, and after that δn_{eff} is calculated for the LP01 mode, where χ_t is the thermo-optic coefficient, evaluated at $8.6*10^{-6}$ by [11].

This thermal drift shows that MZI filters need to be temperature-stabilized when used as passive structures for DPSK demodulation or PSBT optical encoding. Moreover, optical PSBT encoding needs the MZI to remain centered at its transmission peaks. Therefore, if a Mach-Zehnder interferometer is thermally insulated from exterior fluctuations, a second system is needed to maintain the transmission peaks on ITU channels (for the constructive port in both DPSK and PSBT applications). This second adjustment is obtained by applying a supplementary phase shift in one arm, obtained by the heating of one arm of the interferometer.

The implementation of this system must be without mechanical constraints to ensure a low sensitivity of the whole MZI device to polarization effects, usually quantified for optical filters as differential group delay) or PD-λ [12]. PD-λ = polarisation dependent wavelength: specification of the maximal frequency shift between all polarisation states at the input of the component. A second reason justifying the constraint-loss criteria for the heating system is that a large number of expansions/contractions due to the heating could break the interferometer arm.

Description of the 49.5 GHz MZI Used in Section 7

In order to test the all optical PSBT encoding a temperature stabilized MZI must be used. For this application, an accurate temperature stabilisation process has been developed and consists of:

a general regulation circuit which stabilises the temperature for the whole MZI device. This regulation is performed by packaging the MZI device in an aluminium box stabilized with Peltier elements, and after that a local heating system without mechanical constraints to adjust the centre of the MZI on a 50 GHz frequency range.

Figure 13 summarizes the stabilization process: when the exterior temperature (Text) fluctuates, the MZI peaks fluctuate from left to right with a 1.45 GHz/°C drift coefficient.

In (b), the general MZI insulation reduces exterior temperature fluctuation on the MZI; the peaks present no more frequency shifts, but the peak frequencies do not correspond to the ITU frequencies.

In (c), the local heating system produces the phase shift required in one of the MZI arms for the adjustment of the MZI peaks on the ITU grid.

Another important point of the thermal stabilisation pro-cess is the accuracy obtained when the general stabilisation of the MZI is operating (Fig. 13 (b)). In Fig. 14, the evolution of the output power (for a constant wavelength) of the MZI is plotted versus time during the stabilisation process. At first (t ∈ [0;1500] seconds), the output optical power fluctuates with the fluctuation of the MZI package temperature as the MZI spectra shifts from left to right. After that, we can say that when stabilised (after around 2 hours and 20 minutes), the output power remains constant showing a good stabilisation accuracy of the whole MZI ((S) zone in Fig. 14).

Finally, it is also necessary to point out that the fiber temperature can not be measured in the system. Thus, it is the MZI package temperature which is represented in Fig. 14(a). Nevertheless, as the stability criteria of the MZI is the stability of output optical power at a constant wavelength, we can conclude with the Fig. 14(b) that the interferometer is well stabilised.

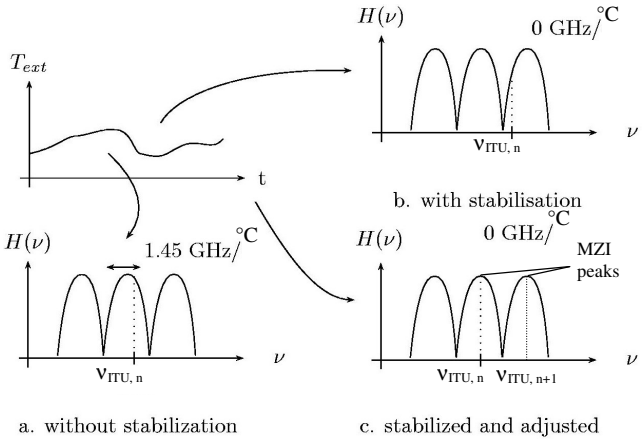

Fig. 13. Thermal stabilization process: no stabilization (a), general regulation (b), and fine adjustment provided by the differential heating system (c). Text is the exterior temperature.

The system is slow but is characterised by good stability over a long stabilisation time. A less than 0.1 °C accuracy has been obtained over many hours and the experiments in section 7 are made during the stabilised state (S). As a conclusion, the MZI is considered to be stabilised enough for experiments. This conclusion can also be justified by the fact that during all experimental measurements presented in section 7 (including possible environmental fluctuations like exterior temperature), the PSBT optical spectra shown in Fig. 22 d remains stable, demonstrating the good stabilization of the MZI.

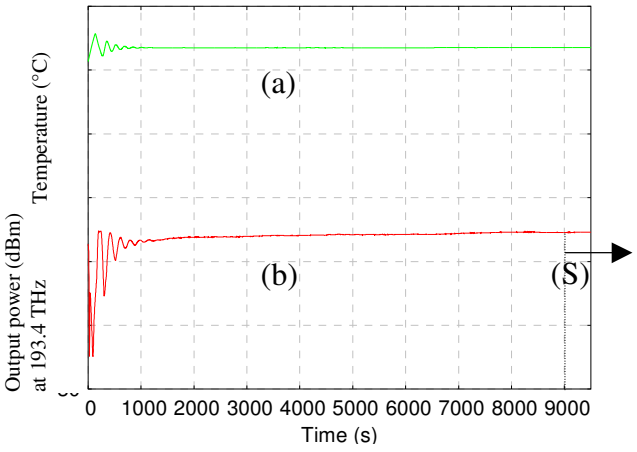

Fig. 14. Thermal stabilization process: (1): temperature of the MZI package and (2): output optical power at 193.4 THz..

By plotting the evolution of the output transmission peak power for an MZI with a 49.5 GHz free spectral range (FSR) (ΔL = 0.41 cm), we determined the thermal periodicity of maximum transmission power. We found a 34.2 °C period, thus giving the drift coefficient 1.45 GHz/°C of the MZI device.

Finally, it is important to note that during the temperature stabilisation process, the FSR remains constant, and a simple calculus can justify this result. For example, we shall consider an MZI with a 50 GHz FSR at 20°C. This MZI will have a delay equal to τ = 20 ps, and a differential length ΔL equal to 4.108 mm. If the temperature increases by ΔT = 50 °C, the TEE will induce a $\Delta L \cdot \Delta T \cdot \alpha_t = 4.108 \cdot 50 \cdot 0.55 * 10^{-6} \approx 1.1 * 10^{-4}$ mm variation on ΔL value. The new value for ΔL at 70 °C will be 4.108 + 0.00011 = 4.10811 mm, thus giving a new delay equal to 20.0005 ps, and an FSR equal to 49.999 GHz. As this reduction of the FSR value is negligible, the FSR can be considered as constant during temperature stabilisation.

5. EXPERIMENTAL CHARACTIRISATION OF THE MZI STRUCTURE

Experimental setup

In this part, some experimental results for characterisation of an all fiber MZI structure are presented. This structure has been realized with commercial 3 dB fused couplers. The MZI has only one output port, and transmission is given by T'_2 in Eq. (19). Our spectral characterisation of the device takes place in ITU 24, 25 and 26 channels. The optical source used here is a DFB WDM laser at 1550.12 nm, and has a 2 nm total tuning range around this wavelength (corresponding to 250 GHz). For transmission spectra measurements, we control the laser wavelength by temperature, and measure the output power. The spectrum is then treated for FSR, differential delay T_b and isolation evaluation. We also use a polarimeter, and the evolution of Stokes parameters (S0, S1, S2, S3, as defined in [13]) of the output field is measured. The PMD of the device is evaluated with the arcsine formula [14]:

$$DGD = \frac{2}{\Delta\omega}.\arcsin\left[\frac{1}{2}.\sqrt{\frac{1}{2}\left(\Delta S_1^2 + \Delta S_2^2 + \Delta S_3^2\right)}\right] \quad (24)$$

Another important parameter of MZI has to be evaluated: the Polarisation Dependent Loss (PDL). The principle is that the transmitted power T'_2 in Eq. (19) is polarisation dependent. The value of PDL is then defined as the difference between maximal and minimal transmissions of the device when describing all the polarisation states for input field. The PDL measurement will be only made in ITU channel 25. Experimental setup is summarized in Figure 15.

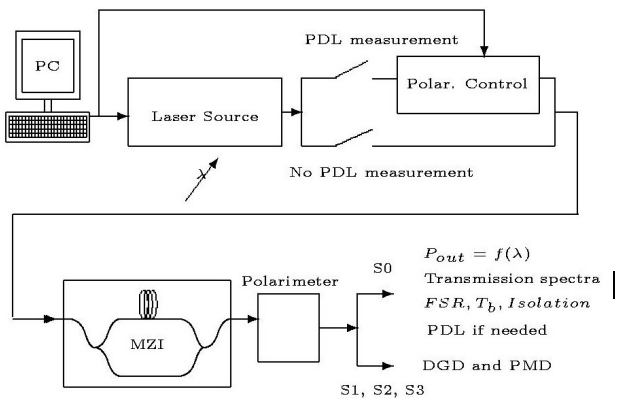

Figure 15. Experimental setup.

Results

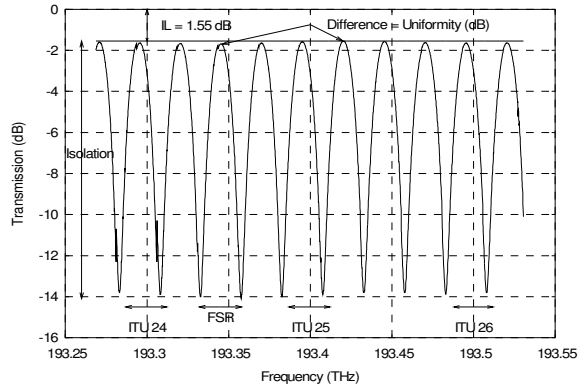

Figure 16. Experimental transmission spectrum of the MZI.

The transmission spectrum of MZI device is plotted on Figure 16. We found an insertion loss IL at 1.55 dB, and an uniformity at 0.1 dB. The isolation ratio is 12.53 dB. The FSR has been evaluated at 26.66 GHz, corresponding to a differential delay T_b at 37.51 ps. The DGD evolution is plotted in Figure 17. Peaks in Figure 17 correspond to destructive interferences in Figure 16, so DGD values are not representative at these wavelengths. Correct DGD values correspond to maximum transmission of MZI, and we found DGD = 5 ps. The PDL of the device has also been evaluated at 0.557 dB.

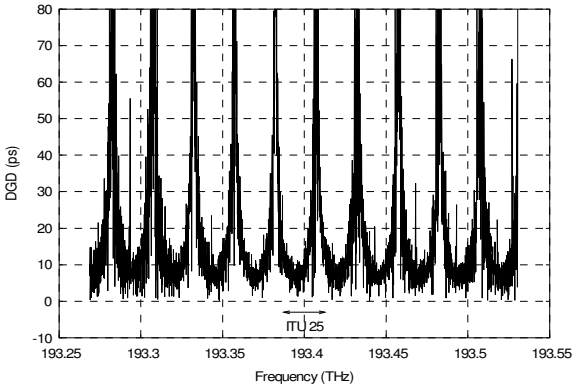

Figure 17. Evolution of DGD of MZI.

Here, the values of DGD (5 ps at minimum) are not acceptable for communications at high data rates (40 Gbps, T_b = 25 ps). A 5 ps PMD value will induce high signal degradations at the reception. High DGD values can be justified by the fact that our MZI is not in a closed box, and is probably made with mechanical constrains.

6. REQUIRED CHARACTERISTICS FOR MZI USED IN DPSK DEMODULATION

Simulated transmission links

Transmitter (Tx): In order to evaluate the required quality for the MZI demodulation devices, we simulated data transmission with 40 Gbps optical links using the DPSK modulation format. The transmitter contains 16 NRZ-DPSK OC-768 channels (40 Gbps), 200 GHz spaced, from 192 to 195 THz (C-band). Optical carriers are gaussian lasers with a 10 MHz FWHM. Data flow is generated by a PRBS (Pseudo Random Binary Sequence) generator (2^9 bits sequence). NRZ pulse shape is gaussian with 10 %.T_b rise/fall times. DPSK signal is obtained with a MZM (Mach-Zehnder Modulator) biased at extinction point. The MZM operates in a push-pull configuration to reduce the chirp [4] and it is characterized with a 30 dB extinction ratio.

Propagation line: The transmission line is composed of a pre-compensation stage, a recirculating loop (50 km/span) and a post-compensation stage to maintain the residual dispersion D.L at 0 ps/nm at the end of the line. The values chosen for the pre and post-compensation D.L correspond to an optimal GVD (Group Velocity Dispersion) compensation [15]. The in-line residual dispersion is equal to $D.L_{res}$ = 20.03 ps/nm, thus giving the lengths of the fiber (the SMF fiber is characterized by D_1 = 17 ps/nm.km and the DCF verifies D_2 = -161.95 ps/nm.km). Dispersion slope coefficients are adjusted for the whole 16 channels grid compensation. Each propagation loop is loss compensated by an EDFA (11.37 dB gain) with a 4.5 dB noise Figure.

Reception device (Rx) : The reception stage is first composed of a gaussian optical filter (80 GHz band pass) for the WDM channel separation. After that, the MZI filter converts the optical DPSK to an NRZ-OOK. The two MZI output's (constructive and destructive) are used in a balanced detection scheme, for OSNR augmentation (theoretically 3 dB [4]).

Non optimal MZI filters suffer from defects located in Figure 17: presence of a differential optical loss α in upper arm and time delay T not equals to the bit duration T_b. Our purpose is to determine the maximal defects leading to an 0.25 dB degraded Q-factor. It corresponds for example to an increase in BER from 10^{-10} to the conventional limit 10^{-9} without FEC (Forward Error Correction). Note that here, we use the conventional Q-factor in the gaussian noise assumption, and therefore all simulated links work in the linear propagation regime. As Q-factor is under-estimated in these cases [16], this criteria is sufficient to ensure a good quality for demodulation.

Results

We reported in table 2 the simulation results obtained. It appears that the delay error (delay error $\Delta_{\%}$ = 1-T/Tb) must remain below 1.8 % to limit eye degradations. This tolerance can be easily linked to the FSR tolerance, as $\Delta FSR = \Delta_{\%}.FSR$, leading to an 1.8 % precise FSR. We also found that minimal isolation required after 900 km propagation is 12.1 dB. This value ensures that the OSNR of the DPSK demodulated signal will be sufficient to avoid eye degradation at the reception.

Link length (km)	0	300	600	900
Isolation min (dB)	25	13.8	12.1	12.1
Delay error (%)	1.8	1.8	2.2	2.2

Table 2: Required characteristics for the MZI used as DPSK demodulator (at 0,25 dB Q penalty)

As the isolation is linked with the upper arm insertion loss (α_{dB}) and with defects in coupling ratios (a_i/b_i), it is interesting to link the minimal isolation required to the maximal optical loss acceptable in the MZI. Assuming ideal couplers (50/50 coupling ratios), we found an "allowable" loss in upper arm of 2.2 dB. This result will have a direct impact on the MZI fabrication: the maximal differential loss between arms will have to be less than 2.2 dB.

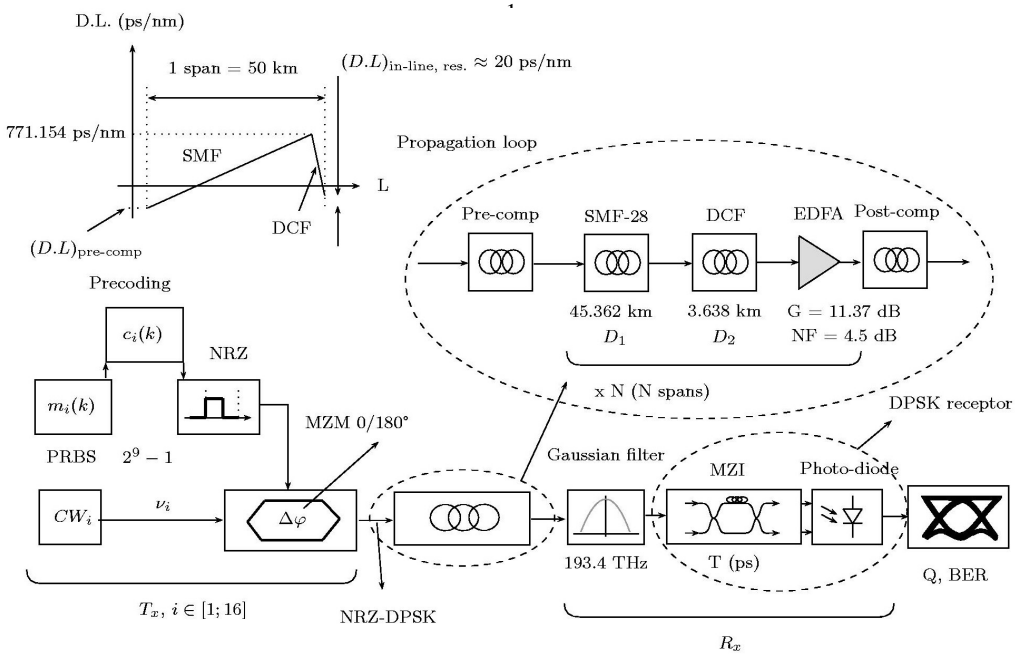

Figure 18: Transmission system: Tx, Propagation loop and Rx.

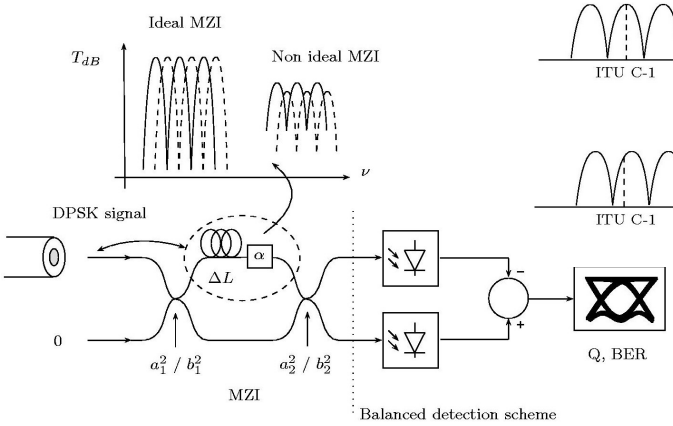

Figure 19: Defects located in the DPSK reception device.

FSR precision required in WDM operation

As DPSK modulation format is well used in WDM configurations [16], the MZI must be operational for multiple wavelengths. Therefore, the tolerance on the FSR precision has to be reconsidered for an MZI working on a ITU WDM grid. For example, let's consider an MZI centered in the 193.4 THz channel (ITU C-25) with a 39.92 GHz FSR ($\Delta\%$ = 0.2 % with OC-768). It is easy to show that the ITU C-49 channel (195.8 THz) will not be operational: first, ITU C-49 and ITU C-25 are separated by 2.4 THz = 60*40 GHz. As the MZI's FSR is equal to 39.92 GHz, the frequency shift between the MZI peak and the ITU C-49 channel will be 60*0.08 GHz = 4.8 GHz as shown in Figure 20. Finally, the C-49 channel will suffer from dB insertion loss (I.L.) and the BER will be higher than in the C-25 channel.

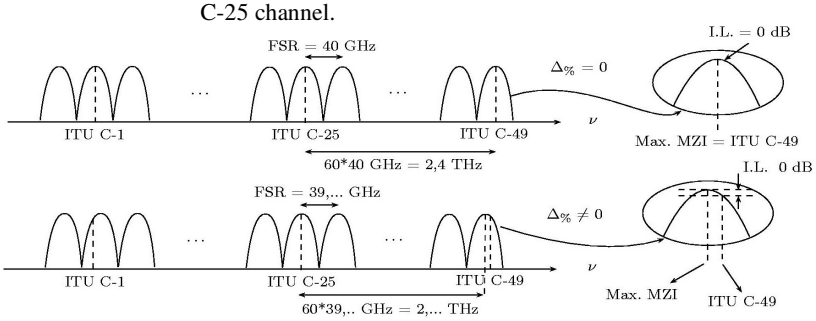

Figure 20: Effect of a non precise FSR ($\Delta_{\%} \neq 0$) on the adjacent WDM channels demodulation: a insertion loss (I.L.) appears, due to the difference between ITU frequency and MZI local transmission peak

The limitation of the adjacent channels insertion loss can be obtained by an accurate FSR, equivalent to a very small value for $\Delta\%$. Values as small as 0.05 % lead to a satisfying demodulation on the whole ITU C-grid. To conclude with this aspect, a 0.05 % tolerance for the FSR leads to an FSR accuracy equals to 0.0005*40 = 20 MHz. This value is suitable to avoid insertion loss the channel located at the extremities.

7. SYSTEM IMPLEMENTATION OF PSBT AND REQUIRED THERMAL CHARACTERISTICS FOR MZI USED IN PSBT ENCODING

System implementation of an all-fiber MZI

PSBT format is usually generated by applying a three levels electrical data signal obtained by electrically filtering a precoded (same as for DPSK format) NRZ data signal to a Mach-Zehnder modulator biased at the minimum of its transfer

function. Depending on modulators characteristics, dual drive or single drive operation can be implemented. In all cases, such a scheme requires excellent linearity of the electrical drivers over a wide frequency range. An optical alternative to the electrical generation of PSBT format has been proposed in [9] by applying an optical filtering function over an optical DPSK 43 Gbps signal.

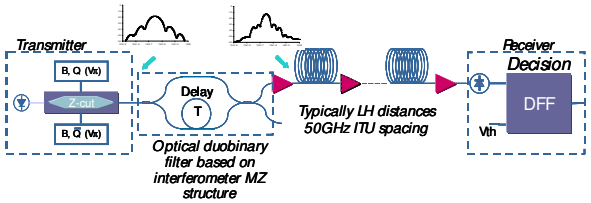

Figure 21: Experimental set-up.

Figure 21 shows the experimental set-up used for experimental demonstration. The optical data output resulting from this set-up is a DPSK format. In order to convert it into PSBT format, the optical data stream is launched into a MZI, in which the differential delay of one arm to the other need to remain between 0.8 to 0.9 bit time. When appropriately tuned using differential heating of the arms, this can ensure 50.0 GHz periodicity for ITU WDM compliance. It has a Frequency Spectral Range of 49.5GHz and is temperature-stabilized.

At the receiver side, an opto-electronic conversion is done by launching the optical signal into a 40 Gbps UTC photodiode matched to a high sensitivity DFF. The 3R regenerated electrical signal at 43 Gbps is then demultiplexed into four 10 Gbps tributaries on which the BER measurement are performed.

The all-fiber MZI is characterized by the values given in Table 3. In this table, the isolation ratio is the interference contrast of the interferometer, and the uniformity is the maximal power difference between the MZI transmission peaks. Moreover, the FSR value of the MZI used in the experiments is 49.5 GHz and not 50 GHz. Such an FSR gives $\tau = 0.86 \cdot Tb$ but this is sufficient for the creation of the PSBT effect.

Isolation (dB)	25
Uniformity (dB)	0.4
DGD (ps)	0.5
Delay (ps)	20.2
FSR (GHz)	49.5

Table 1. Characteristics of the 49.5 GHz fiber-fused interferometer used.

Results

The DPSK optical eye diagram and spectrum obtained at the output of the low-V_π $LiNbO_3$ modulator in front of the optical fiber-based interferometer is shown on Figure 22 a and 22 b.

At the output of the optical filter, a clearly open NRZ-like duobinary eye diagrams (Fig. 22 c) is obtained and a optical spectrum of reduced size (Fig 22 d) is observed.

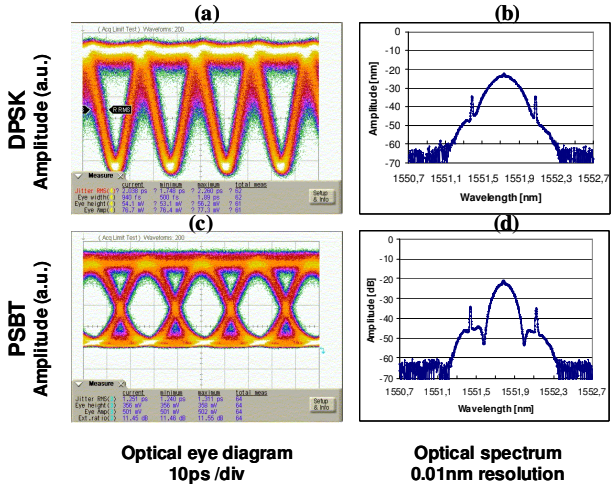

Figure 22 : Optical eye diagram and spectrum at input (a) and output (b) of the fiber based Mach-Zehnder interferometer.

The PSBT format is known for its robustness to Chromatic Dispersion (CD). Due to the NRZ-like appearance of the eye diagram of this optically-generated PSBT format, a reduced robustness to CD with respect to the electrically-generated PSBT format is expected. Figure 23 shows the CD range robustness evolution versus measured Q-factor for 2 values of OSNR penalties and for both optical and electrical PSBT format. Even though the optically-generated PSBT is found – as expected – nearly twice less dispersion tolerant than its electrical counterpart, it remains significantly more robust than NRZ format (100 ps/nm vs. 65 ps/nm at Q=12.6 dB -10^{-5} BER- for 1dB OSNR penalty).

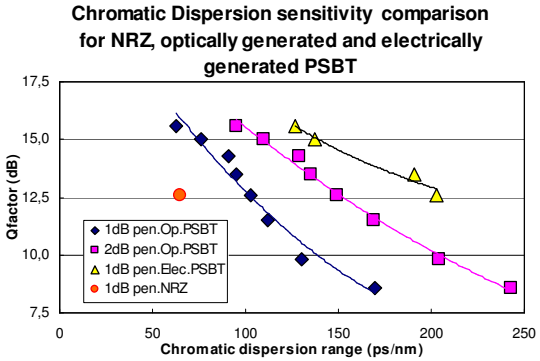

Figure 23 : Chromatic dispersion sensitivity range versus Q-factor.

Thermal accuracy required for MZI used in PSBT transmitters

In order to evaluate the effect of inaccurate thermal stabilization, resulting in a frequency shift in the MZI peak frequencies, we used the 49.5 GHz fiber-fused interferometer described in the preceding sections, which contains an accurate thermal stabilization (precision < 0.1 °C, ensuring an MZI spectral stabilization better than 0.14 GHz).

The laser used (193.2 THz, ITU C-23) was frequency adjusted to create the detuning which is the difference between the laser frequency and the MZI frequency peak value. We studied the evolution of BER (back to back measurements: fiber length = 0

km) with the laser frequency value. Results were plotted as in Fig. 24.

We observed that, as could be expected, the detuning values directly affect the values of the measured BER. More precisely, low detuning values induce severe degradations of the BER values. For example, for a 24 dB optical signal-to-noise ratio (OSNR) (here equivalent to a 10^{-9} BER value without detuning, point A in Fig. 5), a 2 GHz shift from the optimal value induces a BER that is 10 times higher (point B), and a 5 GHz detuning value leads to the 2.10-6 BER value (point C).

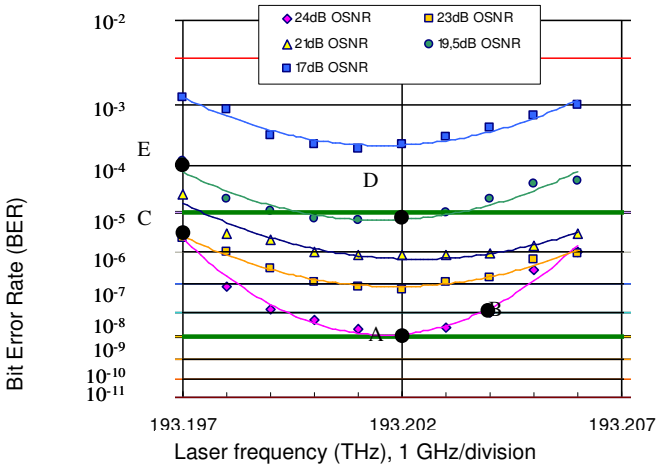

Fig. 24. BER evolution with laser frequency value. Different OSNR values have been considered for these experiments.

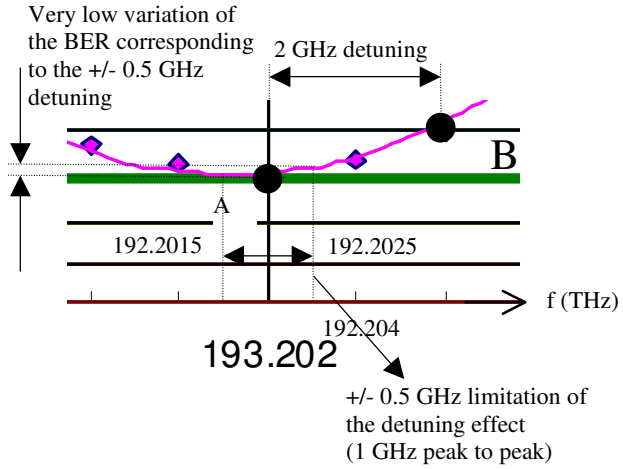

Fig. 25. Enlargement of Fig. 24.

These values are reduced for lower OSNR. At BER $\approx 10^{-5}$ (point D, OSNR = 19.5 dB, no detuning), a 5 GHz frequency shift is enough to degrade the BER by a factor of 10 (point E). The detuning effect appears to be very important, so an inaccurately stabilized MZI will induce large BER fluctuations throughout the whole transmission system.

8. CONCLUSION

DPSK and PSBT have recently been highlighted as suitable modulation formats for 40 Gbps transmissions. The DPSK modulation format presents better performances for transmission than conventional OOK, justifying its utilisation. DPSK needs passives MZIs for interferometric demodulation. PSBT is used for 10 Gbps to 40 Gbps system upgrades, in order to used the already deployed fibers. We have presented the principles of MZI operation in DPSK and PSBT-based systems, with characterisation of useful parameters required for MZI implementation for DPSK demodulation or PSBT encoding.

9. REFERENCES

[1] Jochen Leibrich, Christoph Wree and Werner Rosenkranz, **CF-RZ-DPSK for Suppression of XPM on dispersion Managed Long Haul Optical WDM Transmission on Standard Single Mode Fiber**, IEEE Photonics Technology Letters, vol. 14, No.2, February 2002, pp 155-157.

[2] Chongjin Xie, Lothar Möller, Herbert Haunstein, Stefan Hunsche, **Comparison of System Tolerance to Polarization-Mode Dispersion Between Different Modulation Formats**, IEEE Photonics Technology Letters, vol. 15, No.8, August 2003 pp 1168-1170.

[3] R. Hui., S. Zhang, B. Zhu, R.Huang, C. Allen, D. Demarest, **Advanced Optical Modulation Formats and Their Comparison in Fiber-Optics Systems**, Technical Report, University of Kansas ITTC-FY2004-TR-15666-01, January 2004.

[4] A. H. Gnauck, P. J. Winzer, **Optical Phase Shift-Keyed Transmission**, IEEE J. Lightw. Technol., vol. 23, no. 1, pp. 115-130, January 2005

[5] A. J. Price, L. Pierre, R. Uhel, and V. Havard, **210 km Repeaterless 10 Gb/s Transmission Experiment Through Nondispersion-Shifted Fiber Using Partial Response Scheme**, IEEE Photon. Technol. Lett., vol. 7, No. 10, pp. 1219-1221, October 1995.

[6] D. Penninckx, M. Chbat, L. Pierre et J.P. Thiery, **The Phase-Shaped Binary Transmission (PSBT): A New Technique to Transmit Far Beyond the Chromatic Dispersion Limit**, IEEE Photon. Technol. Lett., vol. 9, no.2, Feb. 1997, pp. 259-261.

[7] T. Ono, Y. Yano, K. Fukuchi, T. Ito, H. Yamazaki, M. Yamaguchi, K. Emura, **Characteristics of Optical Duobinary Signals in Terabit/s Capacity, High-Spectral Efficiency WDM Systems**, IEEE J. Lightw. Technol., vol. 16, no. 5, pp. 788-796, May 1998.

[8] D. Penninckx, M. Chbat, L. Pierre, J. P. Thiery, **Experimental Verification of the Phase Shaped Binray Transmission (PSBT) Effect**, IEEE Photon. Technol. Lett., vol. 10, no.4, April. 1998, pp. 612-614.

[9] P. Brindel, L. Pierre, G. Ducournau, O. Latry, O. Leclerc, M. Ketata, **Optical generation of 43Gbit/s Phase-Shaped-Binary Transmission format from DPSK signal using 50GHz periodic optical filter**, Paper Th 2.2.2, ECOC'05, Glasgow, 2005.

[10] Reinhard März, **Integrated Optics, Design and Modelling**, Artech House Publishers, Boston-London, 1995.

[11] Chang Springfield et al., **Heterodyne Interferometric Measurement of the Thermo-Optic Coefficient of the Single Mode Fiber**, Chinese Journal of Physics, vol. 38, no. 3.I, June 2000, pp. 437-442.

[12] S. Cao, J. Chen, J. N. Damask, C. R. Doerr, L. Guiziou, G. Harvey, Y. Hibino, H. Li, S. Suzuki, K. Y. Wu, and et P. Xie, **Interleaver Technology: Comparisons and**

Applications Requirements, IEEE Journal of Lightwave Technology, Jan. 2004, vol. 22, no. 1, pp. 281-289.

[13] J.P. Gordon and H. Kogelnik, **PMD fundamentals: Polarisation mode dispersion in optical fibers**, Review, PNAS, vol. 97, no. 9, April 25, 2000, pp. 4541, 4550.

[14] Normand Cyr, Bernard Ruchet, Andre Girard and Gregory Schinn, **Poincarre sphere analysis: application to PMD measurements of DWDM components and fibers**, presented at Sub optic convention, Kyoto, Japan, 2001.

[15] Yann Frignac, Jean-Christophe Antona, Sébastien Bigo et Jean-Pierre Hamaide. **Numerical Optimization of pre- and in-line dispersion compensation in dispersion managed systems at 40 Gbit/s**, ThFF5 paper, OFC 2002.

[16] C. Xu, X. Liu, X. Wei, **Differential Phase-Shift Keying for High Spectral Efficiency Optical Transmissions** IEEE Journal of Select. Topics in Quantum Electronics, vol. 10, no.2, pp. 281-293 March/April 2004.